Biosensors and Bioelectronics 78 (2016) 337–343

Contents lists available at ScienceDirect

Biosensors and Bioelectronics

journal homepage: www.elsevier.com/locate/bios

Enhancement of ethanol–oxygen biofuel cell output using a CNT based nano-composite as bioanode

Farideh Gouranlou, Hedayatollah Ghourchian *

Laboratory of Microanalysis, Institute of Biochemistry & Biophysics, Tehran University, Tehran, Iran

ARTICLE INFO

Article history:
Received 25 August 2015
Received in revised form
14 November 2015
Accepted 23 November 2015
Available online 23 November 2015

Keywords:
Biofuel cell
Nanocomposite
Polydiallyldimethylammonium chloride
Biocatalyst
Carbon nanotubes

ABSTRACT

The present research, describes preparation and application of a novel bioanode for ethanol–oxygen biofuel cells. We applied an enzyme based nanocomposite consisting of polymethylene green as electron transfer mediator, carboxylated-multiwall carbon nanotubes as electron transfer accelerator, alcohol dehydrogenase as biocatalyst and polydiallyldimethylammonium chloride as supporting agent. In the presence of β-nicotinamide adenine dinucleotide as cofactor, and ethanol as fuel, the feasibility of the bioanode for increasing the power was evaluated under the ambient conditions. In the optimum conditions the biofuel cell produced the power density of 1.713 mW cm^{-2} and open circuit voltage of 0.281 V.

1. Introduction

Biofuel cells (BFCs) are alternative energy sources which provide bioenergy for portable devices that require low power density batteries. They are usually using biological material such as enzymes which are renewable and non-polluting catalysts. Depending on the biocatalysts, BFCs offer fuel flexibility and operate devices at room temperature in physiological pH. Generally, these systems oxidize organic fuels and reduce oxygen and convert chemical energy into electricity via biochemical reactions. The very early BFC was planned in the beginning of the 20th century, when M.C. Potter used microbial cells on platinum electrodes to produce electricity (Potter, 1912). In the 1960s, NASA was interested in power generation from human wastes for space shuttles (Clark et al., 1962). Then, in 1964, the first enzyme-based biofuel cell was reported using glucose oxidase (GOx) as anodic catalyst and glucose as fuel. However, NAD-dependent alcohol dehydrogenase (NAD-ADH), which catalyzes the oxidation of ethanol, was noticed from different point of views (Liao and Chen, 2001; Sokic-Lazic and Minteer, 2008; Palmore et al., 1998). Akers by immobilizing ADH on a tetra n-butyl ammonium bromide modified Nafion, could improve the power density to 1.16 mW m^{-2} (Akers et al., 2005). Aquino Neto by using the polyamidoamine dendrimer as supporting material for electrostatic layer by layer immobilization of ADH could achieve an acceptable mechanical stability and better control of enzyme disposition for the BFC (Aquino Neto et al., 2011). Several reviews published in recent years cover the newest developments and the different challenges that the scientists in this area are facing (Aquino Neto and de Andrade, 2013; Hao and Scot, 2010). The key point in bioenergy production using NAD-dependent enzymes such as ADH is to regenerate the NAD^+ species and restore the enzymatic cycle (Sokic-Lazic and Minteer, 2008). Direct oxidation of NADH at conventional electrodes, such as gold, platinum, and carbon occurs at extensive over voltage (> 1.0 V), with passivation of the electrode surface (Wu et al., 1996). To solve this problem the electrodes surfaces were modified with multi-walled carbon nanotubes (MWCNTs). MWCNTs mediate the electrocatalytic oxidation of NAD-dependent enzymes (Zhang et al., 2007), diminishing the high overvoltage for NADH oxidation (Shin et al., 2012). The nanosize dimension of CNTs allows them to come toward the active center of biomolecules more closely, favoring electron transfer (Liu and Cai, 2007). Functionalizing the CNTs improves their electronic communication with either the electrode or enzyme. This could be occurred at the end of CNTs via oxygenated species (Yuan et al., 2011). Besides decreasing the over voltage of NAD^+/NADH system, modification of electrode by CNTs enhances the efficiency of enzyme in power density and electron transfer kinetics (Mei et al., 1996). Polydiallyldimethylammonium chloride (PDDA) is a normal and water soluble cationic polyelectrolyte, which has been widely used for the immobilization of biomolecules (Liu and Lin, 2006; Zhao and Ju, 2006; Chen et al., 2007). PDDA usually acts as a

* Corresponding author.
E-mail addresses: fgouranlou@ut.ac.ir (F. Gouranlou), ghourchian@ut.ac.ir (H. Ghourchian).

http://dx.doi.org/10.1016/j.bios.2015.11.064
0956-5663/

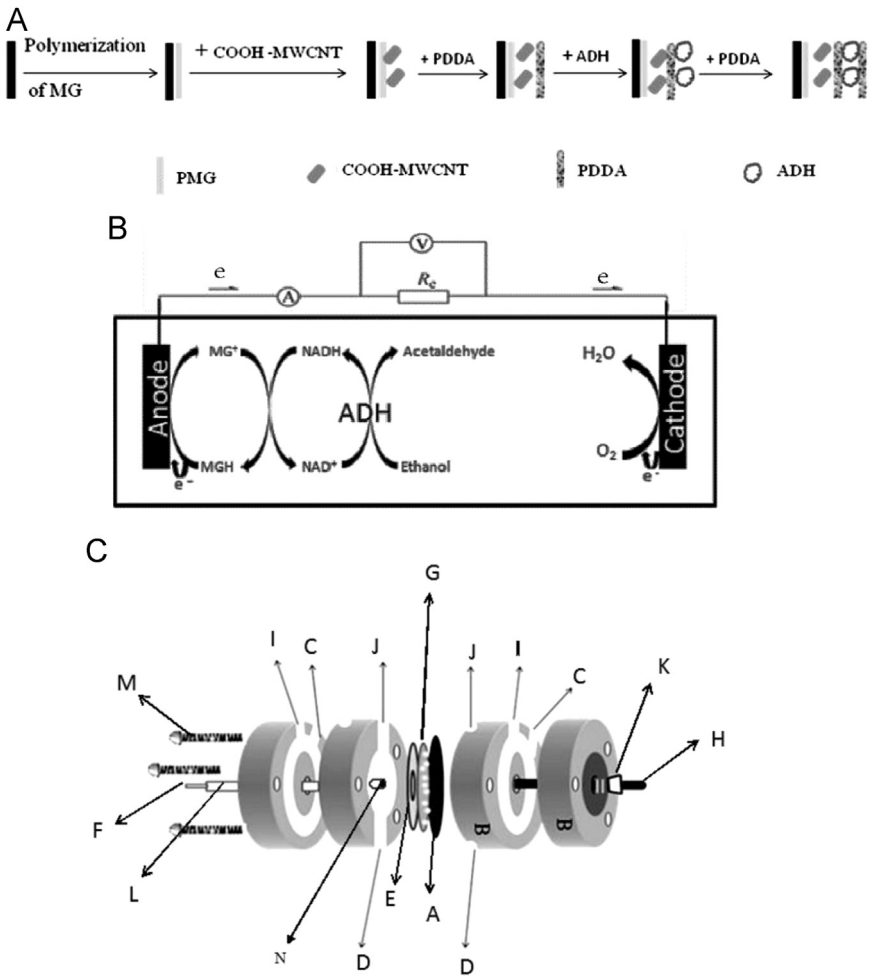

Scheme 1A. Steps for bioanode modification. B: Representations of the anodic and cathodic reactions in ethanol–oxygen biofuel cell. C: Representation of BFC whole cell. (A) Pt/C cathode, (B) Plexiglas body, (C) inlet for water jacket, (D) buffer inlet, (E) septum valve, (F) bioanode connector, (G) perforated Teflon support, (H) graphite connector, (I) outlet for water jacket, (J) buffer outlet, (K) Teflon support for graphite connector, (L) Teflon support for bioanode connector, (M) screw, (N) bioanode.

positively charged colloid when it is dissolved in aqueous solution (Li et al., 2008). This positively charged PDDA can be easily coated on the negatively charged surface by electrostatic interaction (Ensafi et al., 2013). While PDDA can form stable ultra-thin layers on CNTs, it is capable of interacting with negatively charged sites of the enzyme. Obviously, the presence of CNTs supports transport of electrons within the bio-electrocatalytic film.

In the present research, an ADH based nanocomposite is designed in which PDDA is used to disperse the carboxylated multiwall carbon nanotubes (HOOC-MWCNTs) for developing a new bioanode. Since the isoelectric point of ADH lies around 6.8, the negatively charged ADH can adsorb the polycationic PDDA at pH 7.5 via electrostatic interaction. To diminish the overvoltage and improve the BFC efficiency, polymethylene green (PMG) and HOOC-MWCNTs are used. The prepared ADH based nanocomposite in the presence of NAD^+ and ethanol shows a satisfactory power output in comparison to those reported so far.

2. Materials and methods

2.1. Chemicals

ADH (EC. 1.1.1.1) from *Saccharomyces cerevisiae* (lyophilized powder, >300 Units mg^{-1}) and NAD^+ were purchased from Sigma-Aldrich, USA. Sodium phosphate dibasic (Na_2HPO_4), dimethylformamide, sodium phosphate monobasic monohydrate ($NaH_2PO_4.H_2O$), sodium tetraborate ($Na_2B_4O_7$), sodium nitrate ($NaNO_3$), PDDA, ethanol (EtOH) and methylene green (MG) were obtained from Merck, Germany. All the enzyme and coenzyme solutions were freshly prepared and rapidly used. HOOC-MWCNTs ($-$COOH content: 0.49 wt%, outer diameter: 50–80 nm, inner diameter: 5–15 nm, length: 10–20 μm and purity $>95\%$) were acquired from US Research Nanomaterials Inc., USA. All the solutions were prepared with double distilled deionized water.

2.2. Instrumentation

Electrochemical investigations were done using a Potentiostat/Galvanostat EG&G 263 A, Princeton, USA (controlled by a Power Suite software package and a GPIB interface), equipped with a three electrode electrochemical cell including an Ag/AgCl (KCl sat.) as reference electrode, a platinum rod as counter electrode and a glassy carbon (GC, $\varphi=3$ mm, bare or modified with nanocomposite film) from Azar Electrode (Uromia, Iran) as working electrode. Surface morphological studies were carried out using Hitachi S4160 field emission scanning electron microscope, Japan (FESEM) with 10–20 nm gold deposition layer thickness and 30 kV voltages. All the electrochemical measurements were carried out at room temperature and pH was measured using a pH electrode coupled to a Metrohm (Herisau, Switzerland) model 691 pH meter.

2.3. Electrochemical polymerization of methylene green

The GC electrode was polished with 0.3 and 0.05 μm alumina slurry and sonicated in water and ethanol, respectively. Electrochemical polymerization of MG was carried out according to the method described by Zhou et al. (2010).

2.4. Bioanode preparation

For ADH immobilization, at first 1 mg of HOOC-MWCNTs was dispersed in 1 mL of dimethylformamide by using ultrasonic bath to form a black suspension. The PMG modified glassy carbon (GC) electrode was further modified by dropping 2 μl of the prepared HOOC-MWCNTs suspension and drying in air. The modification was followed by addition of 2 μl PDDA (0.5% solution in distilled water) and then dried at air. Finally, 2 μl ADH solution (10 mg/mL) in phosphate buffer solution (PBS, pH 7.5, 0.1 M) was dropped on the modified electrode and then it was covered with 0.5% PDDA solution and dried at room temperature. The thus prepared bioanode (PDDA/ADH/PDDA/HOOC-MWCNTs/PMG/GC) was rinsed with 0.1 M PBS pH 7.5 and stored at 4 °C. The steps for preparation of bioanode were represented in Scheme 1A.

2.5. Biofuel cell design

To set up the BFC, the PDDA/ADH/PDDA/HOOC-MWCNTs/PMG/GC electrode was used as bioanode and a platinized carbon sheet (1×1 cm^2, Vulcan XC-72, 2 mg Pt per cm^2 of carbon, abbreviated as Pt/C, from Nu Vant Systems Inc., Indiana, USA) was used as cathode (Scheme 1B). The bioanode and cathode were fixed in a Plexiglas single compartment cell (Scheme 1C). A graphite rod, attached to the cathode sheet, was placed in a screwed Teflon holder and used for adjusting the distance between cathode and bioanode by screwing the holder. The anode was fixed in the chamber by a septum valve. In order to change the three electrodes electrochemical systems in to two electrodes BFC system, both the reference and auxiliary electrodes were connected to the bioanode and also the working electrode was connected to the cathode. For studying the cell performance, oxygen gas was bubbled in PBS containing 1 mM NAD^+ and 1 mM EtOH for 20 min and injected in the cell using a syringe.

3. Results and discussion

3.1. Electropolymerization of methylene green

Fig. 1A represents the cyclic voltammograms (CVs) for the electrochemical polymerization of MG onto the GC electrode for 10 cycles. Three potential regions are significant. According to Akkermans (Akkermans et al., 1999), the first cathodic region begins with the adsorption of MG^+ to the electrode surface and reducing to two forms of neutral MG (one in solid form at zero V and the other in aqueous form at −0.1 V) in a two-electron, single-proton reaction (Zhao and Ju, 2006):

$$MG^+(aq) + H^+ + 2e^- \rightleftarrows MG\,(s) \quad E_p^{reduction} = -0.09\ V \text{ vs. SCE}$$

$$MG^+(aq) + H^+ + 2e^- \rightleftarrows MG\,(aq) \quad E_p^{reduction} = -0.22\ V \text{ vs. SCE}$$

The reduction wave is converted to two peaks that seems to be due to the separation of consecutive $2e^-$ transferring and obtaining a single proton from solution. In the second anodic region (around 0.18 V vs. Ag/AgCl), the adsorbed MG layer is then oxidized and released to the solution. The third region (1.05 V vs. Ag/AgCl) represents those oxidation processes that complete the film

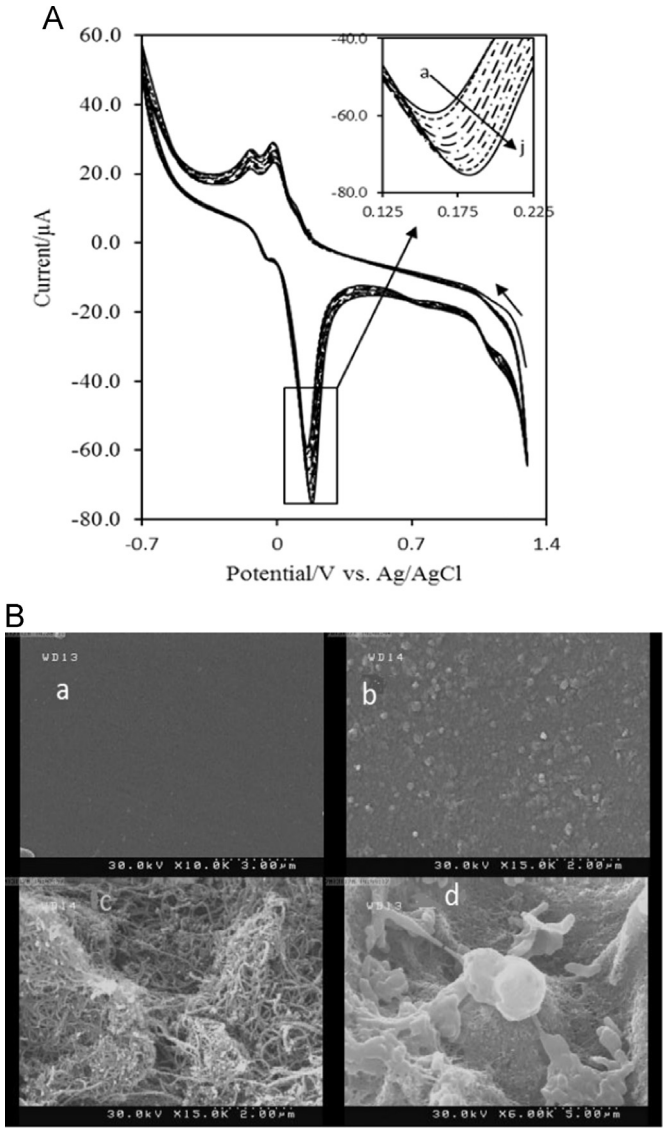

Fig. 1. (A) CVs of MG polymerization on glassy carbon electrode. The experiment was carried out in PBS containing 0.4 mM methylene green, 0.1 M $NaNO_3$ and 10 mM $Na_2B_4O_7$ at the scan rate of 50 mV s^{-1}. The CVs from inner to outer are attributed to the first to 10th cycles. (B) FESEM images of (a) bare GC, (b) PMG/GC; (c) PDDA/HOOC-MWCNTs/PMG/GC and (d) PDDA/ADH/PDDA/HOOC-MWCNTs/PMG/GC electrodes.

grown on the electrode which is related to cycle number (Fenga et al., 2013). More details about the mechanism of MG electrochemical polymerization have been reported elsewhere (Akkermans et al., 1999; Fenga et al., 2013; Karyakin et al 1999a, 1999b). The consecutive cycles in Fig. 1A, represents the progressive process of PMG formation. As shown in Fig. 1A, by increasing the cycle number, the peak currents also increase. At the same time the anodic peak potential shifts to the positive direction and the cathodic peak potential to the negative direction. This could be due to the increase in the quantity of electroactive species on electrode surface and consequently decreases in the rate electron transfer (Yang et al., 1998).

3.2. Surface morphology

Fig. 1B shows the FESEM images of bare GC, PMG/GC, PDDA/HOOC-MWCNTs/PMG/GC and PDDA/ADH/PDDA/HOOC-MWCNTs/PMG/GC electrodes. The image of polymerized PMG is verified by comparing the image of bare GC (Fig. 1B(a)) and that of PMG/GC

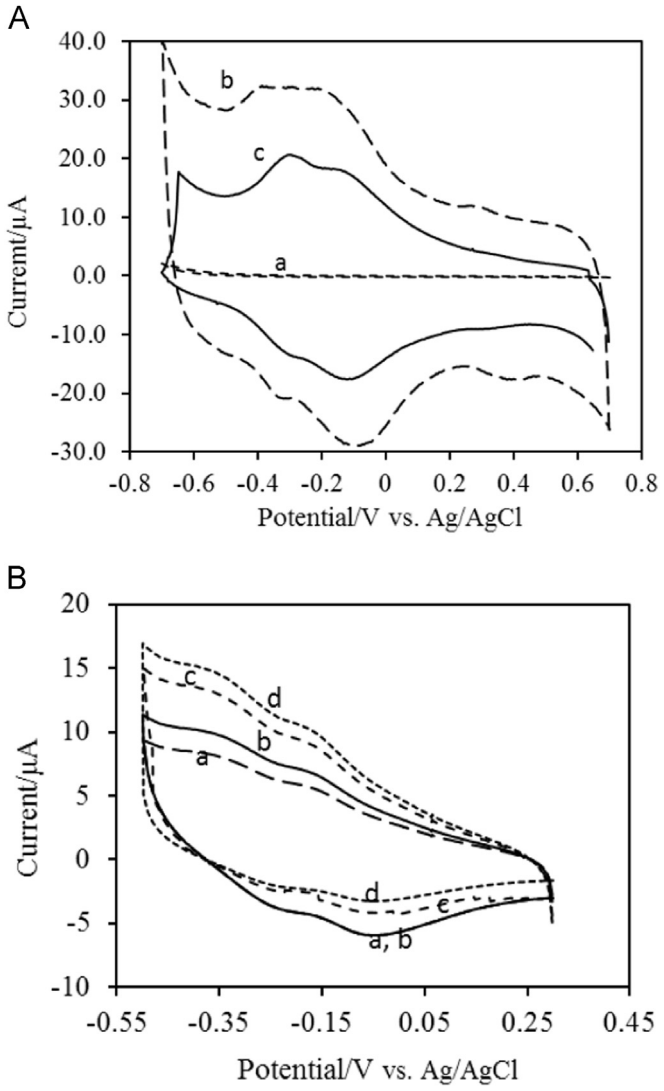

Fig. 2. (A) The CVs of naked GC (a), HOOC-MWCNTs/PMG/GC (b), PDDA/ADH/PDDA/HOOC-MWCNTs/PMG/GC (c) electrodes. The experiment was carried out in PBS (0.1 M, pH 7.5) at scan rate of 50 mV s^{-1}. (B) CVs of different concentrations of NAD^+: (a) 0, (b) 1, (c) 2 and (d) 3 mM at PDDA/ADH/PDDA/HOOC-MWCNT/PMG/GC electrode in PBS (0.1 M, pH 7.5).

(Fig. 1B(b)). A surface-coated layer of CNTs (Fig. 1B(c)) can be clearly differentiated from the uncoated CNTs (Fig. 1B(b)). Comparison between the images of CNTs (Fig. 1B(b)) and that coated by enzyme (Fig. 1B(d)) indicates that ADH is not adsorbed on CNTs as single molecules but it covers the CNTs' surface in agglomerated form so that the overall appearance seems very rough (Moumene et al., 2013; Zebda et al., 2011).

3.3. Electrochemical behavior of nanocomposite

The electrochemical performance of PDDA/ADH/PDDA/HOOC-MWCNTs/PMG nanocomposite on GC electrode in PBS was investigated using cyclic voltammetry. While no peak was observed at the bare GC (Fig. 2A(a)), a well-defined CV was recorded by electropolymerization of MG on naked GC. By adsorbing the HOOC-MWCNTs on PMG, the CV enlarged significantly due to the high conductivity of CNTs (Fig. 2A(b)). It is known that phenazine dyes including carbon nanotube can be easily adsorbed onto the surface of PMG owing to the favorable electrostatic and π–π interactions (Ali and Omanovic, 2013). Coverage of PDDA on HOOC-MWCNTs can shift the cathodic peak to more negative potential and then immobilizing the ADH on PDDA/HOOC-MWCNTs decrease the current peak height that caused by insulating behavior of peptide backbone of enzyme and finally, covering the enzyme with PDDA does not change peak current (Fig. 2A(c)).

The electrochemical behavior of nanocomposite in the presence of NAD^+ was investigated. Fig. 2B showed the CV representing the electrocatalytic activity of modified electrode towards the reduction of NAD^+. PMG is a two-electron mediator which reacts with NAD^+, followed by the regeneration of both PMG and biologically active NADH. Thus, electrochemical response of the modified electrode depends on the reduction of PMG, as given by the following reactions:

$$NAD^+ + PMG_{(red)} \rightarrow NADH + PMG_{(ox)} + H^+$$

$$PMG_{(ox)} + 2e^- \rightarrow PMG_{(red)}$$

As seen in Fig. 2B (curve a) a couple of stable cathodic peaks at −358 and −158 mV vs. Ag/AgCl was observed at modified GC in the absence of NAD^+. However, by addition of NAD^+ an enhancement in cathodic current peak associated with decrease in anodic peak current was observed due to the reduction of NAD^+ to NADH (Fig. 2B).

The electrochemical behavior of nanocomposite in the presence of ethanol was also considered. ADH catalyzes the oxidation of ethanol and simultaneously the cofactor NAD^+ gets reduced to NADH. The reaction that occurred was as follows (Svensson et al., 2005):

$$\text{Ethanol} + NAD^+ \overset{ADH}{\Longrightarrow} \text{Acetaldehyde} + NADH + H^+$$

According to the above reaction, the current from NADH increases with increasing concentration of ethanol, but with adding NADH concentration, the $PMG_{(ox)}$ converts to $PMG_{(red)}$ and at electrode surface, the $PMG_{(red)}$ is changed to $PMG_{(ox)}$ again. Upon addition of ethanol to the solution, the oxidation current increases gently to reach a stable value. The results demonstrate clearly that the electrocatalytic response is very fast and the modified electrode can use as efficient anode in BFC (data not shown).

The amperometric responses of the modified electrode upon additions of 1 mM ethanol to PBS containing 1.0 mM NADH at an applied potential of −0.5 V were shown in Fig. 3A. Upon addition of an aliquot of ethanol to the buffer solution, the reduction current increased steeply to reach a stable value. The results demonstrated clearly that the electrocatalytic response was very fast, which could be used as an efficient ethanol modified electrode. The magnitude of the electric current was proportional to the concentration of ethanol over the range of 1.66–30 μM (Fig. 3B). The effect of pH on ethanol modified electrode lay in two main aspects: the peak potentials and the peak currents. Generally, the optimal pH for enzymes varies based on the immobilization method and microenvironment around them. As seen in Fig. 3C, the maximum current response was obtained at pH 7.5. Fig. 3D shows the plot of potential vs. pH change with the slope of −117 mV pH^{-1}, indicating that two electrons attend in the electron transfer process.

The storage stability of the ADH modified electrode was also examined. When the ADH modified electrode in PBS was stored at 4 °C, it retained 91% and 57.3% of its initial current response for ethanol after two and four weeks, respectively (data not shown). For operational stability, the CV responses of ADH modified electrode were recorded and after 90 continuous cycles the current responses remained ~92% of the original signal.

The reproducibility of electrochemical response for biocathode was examined by CV. The reproducibility of bioanode was determined by comparing 5 modified ADH electrodes. The RSD of ADH modified electrode response toward 1 mM ethanol and 1 mM

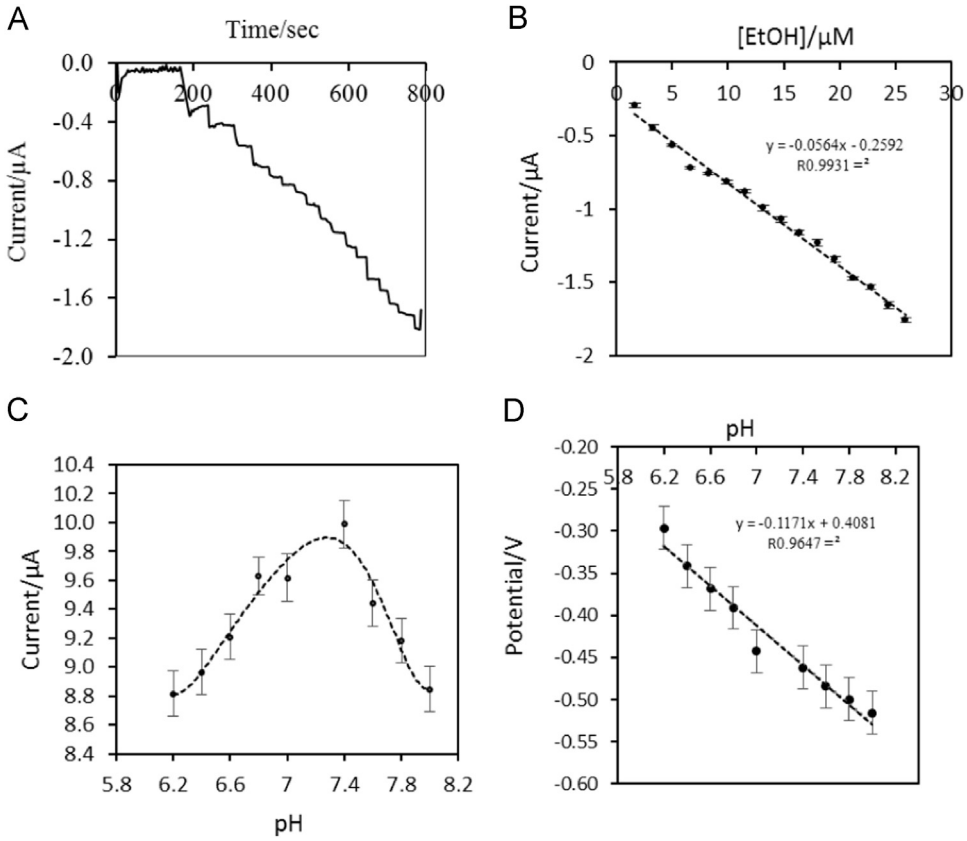

Fig. 3. (A) Chronoamperometric responses of PDDA/ADH/PDDA/HOOC-MWCNTs/PMG/GC electrode toward different concentrations of ethanol (1.66, 3.32, 4.98, 6.62, 8.26, 9.9, 11.53, 13.16, 14.78, 16.39 18.00, 19.61, 21.21, 22.81, 24.39 and 25.94 μM) at the applied potential of −0.5 V (vs. Ag/AgCl). The experiment was carried out in phosphate buffer (0.1 M, pH 7.5) containing 1 mM NAD^+. (B) Current changes against ethanol concentration. (C) Effect of pH on current response. The electrode was inserted in PBS (0.1 M) with different pHs (6.2–7.8) and the CVs were recorded at the scan rate of 50 mV s^{-1}. (D) Potential dependence on pH changes.

NAD^+ in 0.1 M PBS pH 7.5 was 0.97% (data not shown).

3.4. Biofuel cell performance

The BFC is characterized while PDDA/ADH/PDDA/HOOC-MWCNTs/PMG/GC and Pt/C are used as bioanode and cathode respectively and the voltage is measured in oxygen saturated PBS (0.1 M, pH 7.5) containing 1 mM ethanol and 1 mM NAD^+. One of the important parameter in the evaluation of BFCs that will be addressed is open-circuit voltage (OCV), which is the difference of electrical potential between two terminals of a device while disconnected from the circuit and therefore, no external electric current flows between the terminals (Topcagic and Minteer, 2006). The measured OCV is typically less than the theoretical value due to overpotentials at very low current densities. Determination of OCV is necessary for polarization testing. So, the OCV is determined using a Potentiostat/Galvanostat over time until reach to a plateau. The voltage is initially less than 100 mV and then gradually rises to a maximum value of 281 mV. This value is stable at least for 5 h. For polarization testing, the potential is scanned from the OCV value to 0 V at the voltage scan rate of 1 mV s^{-1}.

Fig. 4 represents power and voltage generated in the BFC with respect to current. The produced current density reveals the rate of catalytic turnover and transport processes as a function of the surface area of the electrode. As seen, maximum power density produced by the BFC was 1.713 mW cm^{-2}. The power density of our BFC is higher than those reported in the literature (Table 1). Each polarization curve has three overpotential zones that are related to activation loss, ohmic loss and mass transfer loss which result BFC overpotential (Basu and Basu, 2013; Radoi and Compagnone, 2009). The activation loss is dominant at low current densities when the rate of the electrochemical reaction at the electrode surface is controlled by slow electrode kinetics. The processes comprising adsorption of reactant species, transfer of electrons across the double layer, desorption of product species, the number and distribution of active sites, and the nature of the electrode surface can all contribute to activation loss. Ohmic losses differ directly with current, increasing over the entire range of

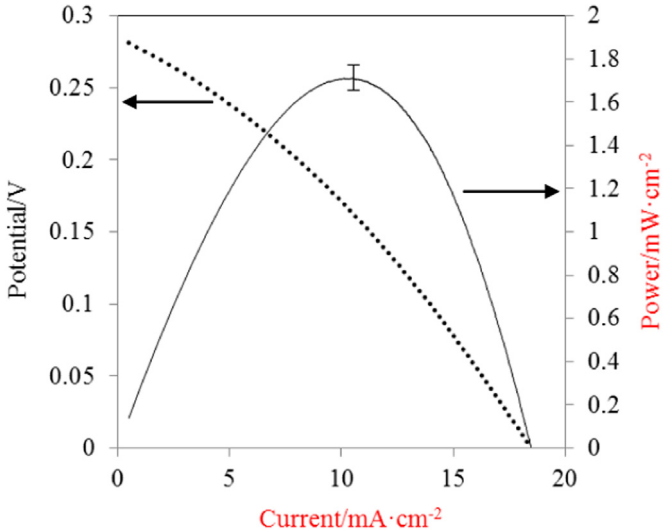

Fig. 4. Polarization curve (dotted line) and power curve (solid line) obtained by the ethanol–oxygen BFC. The experiment was carried out in oxygen saturated PBS (0.1 M, pH 7.5) containing 1 mM ethanol and 1 mM NAD^+. The power density was calculated by multiplying the voltage by the corresponding current density.

Table 1
Comparison of parameters of different BFCs.

Fuel/oxidant	Anode composition	Cathode composition	OCV (V)	Power density ($\times 10^{-6}$ W cm^{-2})	Stability (day)	References
Ethanol/H_2O_2	PAHA-Ru[a]/PDDA/ADH	AOx[b]+MP_8[c]	0.24	1.5s	–	Motoyama et al. (2008)
Ethanol/O_2	ADH/PAMAM[d]/PMG	C–Pt	0.21	63	–	Aquino Neto et al. (2011)
Ethanol/O_2	ADH/PAMAM/PMG	C–Pt	0.45	280	–	Ramanavicius et al. (2008)
Ethanol/O_2, bilirubin	ADH/[Ru(5-phenNH_2)$_3$]$^{2+}$	Bilirubin oxidase	0.45	80	–	Forti et al. (2011)
Ethanol/O_2, bilirubin	ADH/Nafion-TBAB[e]/PMG	Os[f] polymer/Bilirubin oxidase	0.51	390	20	Akers et al. (2005)
Ethanol/O_2	ADH/PMG/ADH/Nafion-TBAB	C–Pt	0.71	1160	5	Murata et al. (2013)
Ethanol/O_2	ADH/TiO_2NTs[g]-TCPP[h]	TTh/TTh[i]	1.13	270	8 h	Zhang et al. (2015)
Ethanol/O_2	ADH/Nafion-TBAB/PMG/MWCNT/Au nanoparticle/PAMAM	C–Pt	0.61	155	21	Aquino Neto et al. (2014)
Ethanol/O_2	ADH/Diaphorase/carbon nanoparticle-polyethyleneimine,(2-methyl-1,4-naphthoquinone)	Nafion/carbon nanoparticle/ABTS[j]/laccase	0.6	90	1	Selloum et al. (2014)
Ethanol/O_2	PMG/HOOC-MWCNTs/PDDA/ADH/PDDA	C–Pt	0.28	1713	30	Present work

[a] 1,10-Phenanthroline-5,6-dione ruthenium complex.
[b] Alcohol oxidase.
[c] Microperoxidase 8.
[d] Polyamidoamine.
[e] Tetrabutyl ammonium bromide.
[f] Osmium.
[g] Hydrothermal prepared TiO_2 nanotubes.
[h] Meso-tetrakis(4-carboxyphenyl) porphyrin.
[i] Electropolymerized 2,2′:5′,2″-terthiophene.
[j] 2,2′-Azino-bis(3-ethylbenzothiazoline-6-sulfonic acid).

current density. These are due to the electrode materials, interconnects current collector plates and constant resistance between various interfaces. The Ohmic losses can be decreased by reducing contact resistances at various interfaces. The concentration losses occur due to the mass transport limitation of reactants/products to or from the electroactive sites. These voltage losses occur over the entire range of current density, but become prominent especially at high currents, when it is difficult to provide enough reactant transferring to the enzyme active sites. But as seen in Fig. 4, only two regions can be distinguished: (a) activation loss in the initial part and (b) ohmic loss and mass transfer loss which are combined in the same zone. For increasing the BFC efficiency, the activation, Ohmic and mass transfer losses should be decreased. The mass transport voltage losses can be reduced by making the higher porosity of the electrode without losing conductivity, or a right combination of the hydrophobic and hydrophilic properties of materials used to construct electrode layer (Deng et al. 2010). The use of HOOC-MWCNTs can decrease all overpotentials because of high electrical conductance and more enzymes loading and therefore promoting the enzyme-substrates interaction (Heller, 2004).

As seen, beside the simplicity of the bioanode preparation, OCV and power density is improved satisfactorily. It seems that PMG as mediator could increase the power generation and cell current because of reducing the redox potential between NAD^+ and electrode and also the existence of HOOC-MWCNTs could increase the electron transferring from substrates to electrode (Motoyama et al., 2008). In addition PDDA provides a biocompatible environment to preserve ADH bioactivity. In the optimum condition the power density test is carried out three times and the standard deviation at maximum power density is calculated to be 6×10^{-5} mW cm^{-2}. The reason for such an increase in power and current density could be attributed to the different parameters: (a) CNTs as efficient hosts for redox species may enhance the electroactivity of bioanode. (b) The large surface area and the electronic conductivity of CNTs may also improve both the reactive species (ADH) loading and electron transfer rate at bioanode, as well. (c) PMG is able to diminish the redox potential of NADH/NAD^+ which accelerate electron transfer rate. (d) CNTs may also accelerate the rate of electron transferring via connecting to the active site of enzyme. (e) Moreover, PDDA may prevent the denaturation of ADH at the surface of CNTs and consequently the enzyme catalyzes more ethanol oxidation. (f) Besides, CNTs increase bioelectrocatalytic processes by offering a closer proximity between the reactive species and the electrode surface, and by improving diffusion of ethanol and oxygen within the enzyme films (Bourourou et al., 2014; Kowalewska and Kulesza, 2012).

4. Conclusion

The large surface area and high electronic conductivity of CNTs are two important factors that improve both the enzyme loading and electron transfer rate. The existence of PDDA as a polyelectrolyte in nanocomposite could keep enough water and other hydrophilic molecules around the enzyme which prolong the ADH activity. In addition, due to some reasons the BFC is so simple which make it more user friendly for commercial applications: (I) It is operating at ambient conditions. (II) The ethanol as fuel is available in fermentation process in low cost. (III) The BFC is non-compartmentalized and does not need to use the membrane. (IV) The design allows the application of BFC directly in a vessel containing alcohol solution (e.g. barrel of wine fermentation). (V) The method for enzyme-immobilization is simple. (VI) The application of MG as mediator decreases the over potential for NAD^+.

Acknowledgment

Financial support provided by the research council of the University of Tehran is gratefully appreciated.

References

Akers, N.L., Moore, C.M., Minteer, S.D., 2005. Electrochim. Acta 50, 2521–2525.
Akkermans, R.P., Roberts, S.L., Compton, R.G., 1999. Chem. Commun. 12, 1115–1116.
Ali, I., Omanovic, S., 2013. Int. J. Electrochem. Sci. 8, 4283–4304.
Aquino Neto, S., Almeida, T.S., Palma, L.M., Minteer, S.D., de Andrade, A.R., 2014. J. Power Sources 259, 25–32.
Aquino Neto, S., de Andrade, A.R., 2013. J. Braz. Chem. Soc. 24 (12), 1891–1912.
Aquino Neto, S., Forti, J.C., Zucolotto, V., Ciancaglini, P., de Andrade, A.R., 2011. Biosens. Bioelectron. 26 (6), 2922–2926.
Basu, D., Basu, S., 2013. J. Solid State Electrochem. 17, 2927–2938.
Bourourou, M., Elouarzaki, K., Holzinger, M., Agnès, C., Le Goff, A., Reverdy-Bruas, N., Chaussy, D., Party, M., Maaref, A., Cosnier, S., 2014. Chem. Sci. 5, 2885–2888.
Chen, X., Yan, X., Khor, K.A., Tay, B.K., 2007. Biosens. Bioelectron. 22, 3256–3260.
Clark, L.C., Lyons Jr., C., Ann, N.Y., 1962. Acad. Sci. 102, 29–45.
Deng, L., Shang, L., Wen, D., Zhai, J., Dong, Sh, 2010. Biosens. Bioelectron. 26, 70–73.
Ensafi, A.A., Amini, M., Rezaei, B., 2013. Sens. Actuators B 177, 862–870.
Fenga, P.G., Cardoso, F.P., Aquino Neto, S., de Andrade, A.R., 2013. Electrochim. Acta 106 (1), 109–113.
Forti, J.C., Aquino Neto, S., Zucolotto, V., Ciancaglini, P., de Andrade, A.R., 2011. Biosens. Bioelectron. 26, 2675–2679.
Hao, E., Scot, Y.K., 2010. Energies 3, 23–42.
Heller, A., 2004. Phys. Chem. Chem. Phys. 6, 209–216.
Kowalewska, B., Kulesza, P.J., 2012. Anal. Chem. 21 (84), 9564–9571.
Karyakin, A.A., Karyakina, E.E., Schmidt, H.L., 1999a. Electroanalysis 11 (3), 149–155.
Karyakin, A.A., Karyakina, E.E., Schuhmann, W., Schmidt, H.L., 1999b. Electroanalysis 11 (8), 553–557.
Li, N., Zhao, H.W., Yuan, R., Peng, K.F., Chai, Y.Q., 2008. Electrochim. Acta 54, 235–241.
Liao, M.H., Chen, D.H., 2001. Biotechnol. Lett. 23, 1723–1727.
Liu, G., Lin, Y., 2006. Electrochem. Commun. 8, 251–256.
Liu, S., Cai, C., 2007. J. Electroanal. Chem. 602, 103–114.
Mei, Z.D., Qun, F.H., Yuan, C.H., Xian, J.H., Yun, W., 1996. Anal. Chim. Acta 329 (1–2), 41–48.
Motoyama, Y., Nakamura, N., Ohno, H., 2008. Electroanalysis 20 (8), 923–926.
Moumene, M., Rochefortand, D., Mohamedi, M., 2013. Int. J. Electrochem. Sci. 8, 2009–2022.
Murata, K., Kajiya, K., Masuda, M., Nakamura, N., Ohno, H., 2013. In: Proceedings of the 213th ECS Meeting, Abstract 226.
Palmore, G.T.R., Bertschy, H., Bergens, S.H., Whitesides, G.M., 1998. J. Electroanal. Chem. 443, 155–161.
Potter, M.C., 1912. Proc. R. Soc. Lond. Ser. B 84, 260–276.
Radoi, A., Compagnone, D., 2009. Bioelectrochemistry 76 (1–2), 126–134.
Ramanavicius, A., Kausaite, A., Ramanaviciene, A., 2008. Biosens. Bioelectron. 24, 761–766.
Selloum, D., Tingry, S., Techer, V., Renaud, L., Innocent, C., Zouaoui, A., 2014. J. Power Sourc. 269, 834–840.
Shin, B., Shin, H., Kang, C., 2012. Bull. Korean Chem. Soc. 33 (12), 4211–4214.
Sokic-Lazic, D., Minteer, S.D., 2008. Biosens. Bioelectron. 24, 939–944.
Svensson, K., Bulowa, L., Kriz, D., Krook, M., 2005. Biosens. Bioelectron. 21, 705–711.
Topcagic, S., Minteer, S.D., 2006. Electrochim. Acta 51, 2168–2172.
Wu, Q., Maskus, M., Pariente, F., Tobalina, F., Fernández, V.M., Lorenzo, E., Abruña, H. D., 1996. Anal. Chem. 68 (20), 3688–3696.
Yang, R., Ruan, C., Deng, J., 1998. J. Appl. Electrochem. 28, 1269–1275.
Yuan, J., Chen, J., Wu, X., Fang, K., Niu, L., 2011. J. Electroanal. Chem. 656, 120–124.
Zebda, A., Gondran, C., Le Goff, A., Holzinger, M., Cinquin, P., Cosnier, S., 2011. Nat. Commun. 2, 1–6.
Zhang, M., Mullens, C., Gorski, W., 2007. Anal. Chem. 79 (6), 2446–2450.
Zhang, L., Bai, L., Xu, M., Han, L., Dong, S., 2015. Nano Energy 11, 48–55.
Zhao, H., Ju, H., 2006. Anal. Biochem. 350, 138–144.
Zhou, H., Zhang, Z., Su, L., Mao, L.,, 2010. Langmuir 20–26 (8), 6028–6032.